Open Access Journal
Journal of Power Technologies 93 (2) (2013) 122–132
journal homepage:papers.itc.pw.edu.pl

Stagnation flow of couple stress nanofluid over an exponentially stretching sheet through a porous medium

Abdul Rehman*, S. Nadeem, M. Y. Malik

Department of Mathematics, Quaid-i-Azam University
45320, Islamabad 44000, Pakistan

Abstract

This paper investigates the problem of boundary layer stagnation point flow and heat transfer of couple stress fluid containing nanoparticles and flowing over an exponentially stretching surface in a porous medium. The governing equations of the couple stress fluid model for velocity, temperature and nanoparticle profiles are given as part of the boundary layer approach. The nonlinear partial differential equations are simplified by using similar transformations. The analytical solutions of simplified equations are found using the homotopy analysis method. The convergence of the HAM solutions is discussed by plotting $\hbar$-curves and also through homotopy padé approximation. The physical features of pertinent parameters are discussed through graphs.

Keywords: Boundary layer flow, Couple stress fluid, Nanoparticles, Porous medium, Exponential stretching/shrinking, Analytical solution

1. Introduction

Fluid flow through porous media has many practical applications in physical and industrial processes. A few commonly used examples include: fiber and granular insulations, thermal insulation of buildings, cores and designs of pebble bed nuclear reactors, winding structures for high power density electric machines, food processing and storage, underground disposal of heavy water. Transport properties of fluid saturated porous materials are very important in the petroleum, and geothermal industries. Underground crushed rock saturated with liquid changes its position through the material under the influence of pressure gradient. Rosali et al. [1] discussed the problem of steady stagnation-point flow and heat transfer of viscous fluid over a shrinking sheet in a porous medium. Subsequently, Liu [2] studied the flow and heat transfer of a steady laminar boundary layer flow of an electrically conducting second grade fluid in a porous medium subject to a transverse and uniform magnetic field over a stretching sheet with power law heat flux. Further, Nadeem and Awais [3] analyzed the influence of variable viscosity and variable thermocapillarity on the unsteady flow and heat transfer in a thin film on a horizontal porous shrinking sheet through porous medium. In another work, Nadeem et al. [4] examined the magnetohydrodynamic effects of unsteady boundary layer flow of a micropolar fluid through a porous medium near a forward stagnation-point of an infinite plane wall. A few other interesting works concerning fluid flow through a porous medium in different situations are referred to in [5–10].

*Corresponding author
Email addresses: rehman_maths@hotmail.com (Abdul Rehman*), snqau@hotmail.com (S. Nadeem), drmymalik@hotmail.com (M. Y. Malik)

Due to the high thermal conductivity of nano sized particles, the study of nano fluids has gained much importance in recent years. Kuznetsov and Nield [11] discussed the problem of natural convection boundary layer flow of a nanofluid past a vertical plate. They also discussed the influence of Brownian motion and thermophoresis over the flow and heat transfer of nanoparticles. In a recent work, Nadeem et al. [12] investigated the problem of boundary layer flow and heat transfer of a nanofluid over a vertical slender cylinder. Moreover, Ahmad and Pop [13] reviewed the problem of mixed convection heat transfer effects over the boundary layer flow from a vertical flat plate embedded in a porous medium filled with nanofluids. The study investigated three specified nanofluids: cuprom, aluminum and titanium. Furthermore, Xuan and Roetzel [14] studied the heat transfer of nanofluids considering single-phase and multi-phase features of nanofluids. Recently, Nadeem et al. [15] surveyed the behavior of nanoparticles for the flow of steady, axisymmetric stagnation-point flow of a micropolar fluid in a moving cylinder. Also, Yang et al. [16] inspected the thermal conductivity and viscosity effects over the flow of nanofluids.

The purpose of the present effort is to observe porosity and nano concentration effects over the flow and heat transfer of boundary layer stagnation flow of a couple stress fluid over an exponentially stretching surface. The study of couple-stress fluids looks at the effects of particle size, which is of particular interest in the study of synthetic fluids, thick polymer oils, liquid crystals and animal blood. Its enhanced lead carrying capacity flow through a thin film is also an important aspect of interest from the industrial point of view [17–20]. Stagnation points refer to the points where static pressure is the maximum. Such type of fluid flows are common in plastic sheet extrusion, cooling of metallic plates, boundary layer along the material surface handling conveyers. To the best of the authors' knowledge nano couple stress fluid is still unexplored. The nonlinear partial differential equations of conservation of mass, momentum, heat transfer and nanoparticle concentration are simplified under boundary layer approximations and similar similarity transformations. The resulting system is then solved with the help of the homotopy analysis method (HAM). The problem is also provided with a numerical solution by using the Runge-Kutta-Fehlberg method, and a comparison of both solutions is also presented. At the end there is a detailed discussion concerning the convergence of the HAM solution, and the influence of the important physical parameters involved is also studied. For a special case, a comparison of the present results with existing work [21] is also presented.

2. Formulation

Let us consider the boundary layer stagnation point flow of a steady incompressible couple stress fluid over an exponentially stretching sheet through a porous medium. The Cartesian coordinates (x, y) are used such that x is along the surface of the sheet, while y is taken normal to it. In the presence of the nanoparticles the boundary layer equations of conservation of mass, momentum, heat transfer and concentration applicable for dilute solutions of nanofluids are

$$u_x + v_y = 0, \tag{1}$$

$$uu_x + vu_y = U_\infty \frac{dU_\infty}{dx} + \nu_c u_{yy} - \frac{\eta_0}{\rho} u_{yyyy} - \frac{\nu_c \phi_p^*}{k_0} u, \tag{2}$$

$$uT_x + vT_y = \alpha T_{yy} + \frac{\rho^* c_p^*}{\rho c_p} \left(D_B T_y \phi_y + \frac{D_T}{T_\infty} T_y^2 \right), \tag{3}$$

$$u\phi_x + v\phi_y = D_B \phi_{yy} + \frac{D_T}{T_\infty} T_{yy}, \tag{4}$$

here (u, v) are the velocity components along the (x, y) axes, ν_c is the kinematic viscosity, U_∞ is the free-stream velocity, η_0 is the material constant for the couple stress fluid, ρ is the density, ϕ_p^* is porosity of porous space, k_0 is permeability of porous space, T is temperature, α is the thermal diffusivity, c_p is the specific heat at constant pressure, $\rho^*$is the nanoparticle mass density, c_p^* is the effective heat of the nanoparticle material, ϕ is the nanoparticle volume friction, D_B is the Brownian diffusion coefficient and D_T is the thermophretic diffusion coefficient. The corresponding boundary conditions for the problem are

$$\begin{array}{c} u = U_w, \quad v = 0, \quad at\ y = 0, \\ u \to U_\infty, \quad as\ y \to \infty, \end{array} \tag{5}$$

$$u_{yy} = 0, \quad at\ y = 0, \quad and \quad u_y = 0, \quad y \to \infty, \tag{6}$$

$$\begin{array}{c} T = T_w(x), \quad \phi = \phi_w(x) \quad at\ y = 0, \\ T \to T_\infty, \quad \phi \to \phi_\infty, \quad y \to \infty, \end{array} \tag{7}$$

where the free-stream velocity U_∞, the stretching velocity U_w and the surface temperature T_w are defined as

$$U_\infty = ae^{x/L}, \quad U_w = be^{x/L}, \quad T_w = T_\infty + ce^{x/L}, \tag{8}$$

where a, b and c are constants with appropriate dimensions while L is the reference length.

3. Solution of the problem

For solution of the problem we take the following similar similarity transformations [21]

$$\begin{array}{c} u = ae^{x/L} f'(\eta), \\ v = -\left(\frac{\nu_c a}{2L}\right)^{1/2} e^{x/L} \left(f(\eta) + \eta f'(\eta)\right), \end{array} \tag{9}$$

$$\theta = \frac{T - T_\infty}{T_w - T_\infty}, \quad \psi = \frac{\phi - \phi_\infty}{\phi_w - \phi_\infty}, \tag{10}$$

$$\eta = \left(\frac{a}{2\nu_c L}\right)^{1/2} e^{x/2L} y. \tag{11}$$

With the help of transformations in Eqs. (9) to (11), Eq. (1) is identically satisfied while Eqs. (2) to (4) take the form

$$\lambda f^{(5)} - f''' - ff'' + 2f'^2 - 2 + k_p f' = 0, \tag{12}$$

$$\theta'' + Pr\left(f\theta' - 2f'\theta\right) + N_b\theta'\psi' + N_T\theta'^2 = 0, \tag{13}$$

$$\psi'' + Pr\,Le\left(f\psi' - 2f'\psi\right) + \frac{N_T}{N_b}\theta'' = 0, \tag{14}$$

where $\lambda = \eta_0 U_\infty / 2\mu\nu_c L$ is the couple stress parameter, $k_p = 2\nu_c L\phi_p^* / U_\infty k_0$ is the porosity parameter, $Pr = \nu_c/\alpha$ is the Prandtl number, $N_b = (\phi_w - \phi_\infty)\, D_B \rho^* c_p^* / \alpha\rho c_p$ is the Brownian number, $N_T = (T_w - T_\infty)\, D_T \rho^* c_p^* / \alpha\rho c_p T_\infty$ is the thermophoresis number and $Le = \alpha/D_B$ is the Lewis number. The boundary conditions in nondimensional form are

$$f(0) = 0, \quad f'(0) = \varepsilon, \quad f'''(0) = 0, \tag{15}$$

$$f' \to 1, \quad f'' \to 0, \quad as\ \eta \to \infty, \tag{16}$$

$$\theta(0) = 1, \quad \psi(0) = 1, \quad \theta \to 0, \quad \psi \to 0\ as\ \eta \to \infty, \tag{17}$$

where $\varepsilon = b/a$ is the stretching ratio. To solve the problem with the help of homotopy analysis method (HAM), the initial guess chosen and the corresponding auxiliary linear operators are [22–26]

$$\begin{array}{c} f_0 = (\varepsilon - 1) + (\varepsilon - 1)\left(\frac{\eta^2}{6} - 1\right)e^{-\eta} + \eta, \\ \theta_0 = e^{-\eta}, \quad \psi_0 = e^{-\eta}, \end{array} \tag{18}$$

$$L_f = \frac{d^5}{d\eta^5} + 3\frac{d^4}{d\eta^4} + 3\frac{d^3}{d\eta^3} + \frac{d^2}{d\eta^2}, \tag{19}$$

$$L_\theta = \frac{d^2}{d\eta^2} + \frac{d}{d\eta}, \quad L_\psi = \frac{d^2}{d\eta^2} + \frac{d}{d\eta}. \tag{20}$$

The 0^{th}-order deformation equations are

$$(1 - q)\, L_f\left[\hat{f}(\eta; q) - f_0(\eta)\right] = qH_f\hbar_1 N_f\left[\hat{f}(\eta; q)\right], \tag{21}$$

$$(1 - q)\, L_\theta\left[\hat{\theta}(\eta; q) - \theta_0(\eta)\right] = qH_\theta\hbar_2 N_\theta\left[\hat{\theta}(\eta; q)\right], \tag{22}$$

$$(1 - q)\ L_\Psi\left[\hat{\Psi}(\eta; q) - \Psi_0(\eta)\right] = qH_\Psi\hbar_3 N_\Psi\left[\hat{\Psi}(\eta; q)\right] \tag{23}$$

Where $q \in [0,\ 1]$ is the embedding parameter, $\hbar_1$, $\hbar_2$, $\hbar_3$ are the auxiliary parameter that play an imperative rule for convergence of the HAM solution and H_f, H_θ, H_Ψ are the auxiliary functions.

$$N_f\left[\hat{f}(\eta;\ p)\right] = \lambda\hat{f}^{v} - \hat{f}' - \hat{f}\hat{f}'' + \hat{f}'^2 - 2 + k_p\hat{f}', \quad (24)$$

$$N_\theta\left[\hat{\theta}(\eta;\ q)\right] = \hat{\theta}'' + Pr\left(\hat{f}\hat{\theta}' - 2\hat{f}'\hat{\theta}\right) + N_b\hat{\theta}'\hat{\Psi}' + N_t\hat{\theta}'^2, \quad (25)$$

$$N_\Psi\left[\hat{\Psi}(\eta;\ q)\right] = \hat{\Psi}'' + Le\,Pr\left(\hat{f}\hat{\Psi}' - 2\hat{f}'\hat{\Psi}\right) + \frac{N_t}{N_b}\hat{\theta}''. \quad (26)$$

Further details of the HAM solution are presented in the results and discussion section. The important physical quantities heat flux at the surface of the sheet q_w, the local Nusselt numbers Nu and the Sherwood number Sh associated with the present problem are

$$q_w = -k\frac{\partial T}{\partial y}|_{y=0}, \quad Nu_x = -\sqrt{Re_x}\theta'(0), \quad Sh = -\sqrt{Re_x}\psi'(0), \quad (27)$$

where $Re_x = U_\infty x^2/2\nu L$.

4. Results and discussion

The problem of boundary layer stagnation flow and heat transfer of a couple stress nanofluid flowing over an exponentially stretching sheet through a porous medium is solved analytically using the homotopy analysis method (HAM). The reliability and convergence of HAM solutions are examined by computing $\hbar$-curves for nondimensional velocity, temperature and nanoparticle profiles f', θ and ψ.
The figures are computed for the 15^{th} order of HAM approximations. Further, the homotopy padé approximation is also applied to confirm the convergence of the solutions, while for the validity of our solutions, a comparison of the HAM solutions is tabulated with the numerical solutions obtained through the Runge-Kutta-Fehlberg method. Moreover, a special case of the present work is also compared with the available work [21]. Figs. 1 to 3 are planted to observe the convergence regions of the involved auxiliary parameters $\hbar_1$, $\hbar_2$ and $\hbar_3$ for nondimensional velocity, temperature and nanoparticle profiles and

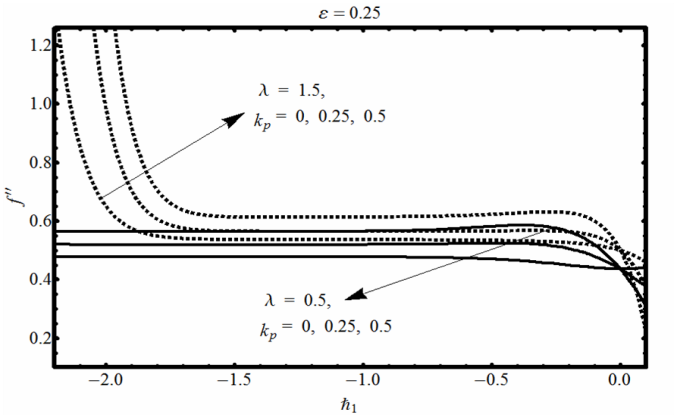

Figure 1: $\hbar$- curves for f' for different values of λ and k_p plotted at 15^{th}-order of approximation

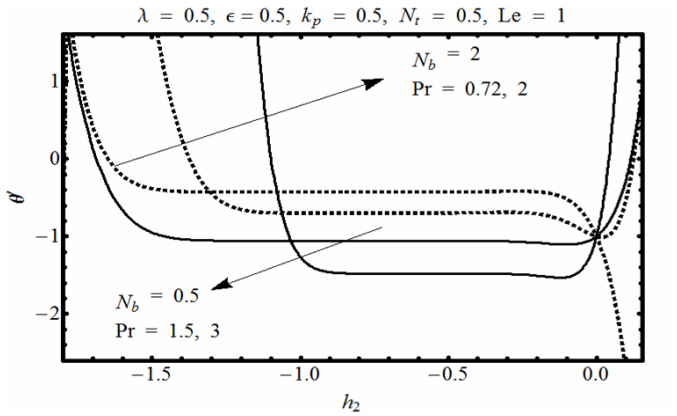

Figure 2: $\hbar$- curves for temperature profile θ for different values of N_b and Pr, plotted at 15^{th}-order of approximation

for different combinations of the other involved parameters. Fig. 1 is sketched for the convergence regions of the velocity profile for different combinations of couple stress parameter λ, porosity parameter k_p when stretching parameter $\varepsilon = 0.25$. It is noticed that an increase in both λ and k_p decreases the acceptable convergence region for the auxiliary parameter $\hbar_1$. From Fig. 1 the convergence region for the velocity profile with $\lambda = 1.5$ and $k_p = 0.5$ is $-1.1 \le \hbar_1 \le -0.3$. Fig. 2 contains the $\hbar$-curves plotted against the temperature gradient for different Prandtl numbers Pr and N_b, while Fig. 3 gives the $\hbar$-curves for the nanoparticle profile for different values of Pr and Le. From Figs. 2 and 3 increase in Pr, N_b and Le decreases the convergence region. From Fig. 3 when $Le = 0.5$ and $Pr = 5$, the acceptable convergence region for the auxiliary parameter is $-1.2 \le \hbar_3 \le -0.2$.

Table 1: Padé table showing the convergence of velocity, temperature and nanoparticle profiles for $\hbar_1 = \hbar_2 = \hbar_3 = -1$, $Pr = 0.72$, $\lambda = 1$, $k_p = 0$, $N_b = 1$, $N_T = 1$, $Le = 1$

Order of App.	$f''(0)$	$\theta'(0)$	$\psi'(0)$	Order of App.	$f''(0)$	$\theta'(0)$	$\psi'(0)$
[1/1]	0.4883	-0.7601	-1.1705	[10/10]	0.4579	-0.7434	-1.1297
[2/2]	0.4814	-0.7449	-1.1274	[11/11]	0.4579	-0.7434	-1.1297
[4/4]	0.4611	-0.7438	-1.1282	[13/13]	0.4578	-0.7433	-1.1298
[5/5]	0.4591	-0.7436	-1.1288	[15/15]	0.4578	-0.7433	-1.1298
[7/7]	0.4582	-0.7435	-1.1294	[18/18]	0.4578	-0.7433	-1.1299
[8/8]	0.4580	-0.7434	-1.1295	[20/20]	0..4578	-0.7433	-1.1299

Table 2: Comparison of numerical and HAM solutions for the boundary derivatives f''

	$-f'(0)$							
	HAM	Fehlberg	HAM	Fehlberg	HAM	Fehlberg	HAM	Fehlberg
$\lambda \backslash k_p$	0		0.5		1		2	
0.5	1.2161	1.2161	1.3640	1.3640	1.4977	1.4977	1.7280	1.7280
1.0	1.0622	1.0622	1.1909	1.1909	1.3070	1.3070	1.5061	1.5061
1.5	0.9771	0.9771	1.0953	1.0953	1.2019	1.2019	1.3841	1.3841
2.0	0.9194	0.9194	1.0304	1.0304	1.1306	1.1306	1.3017	1.3017
5.0	0.7513	0.7513	0.8418	0.8418	0.9235	0.9235	1.0631	1.0631

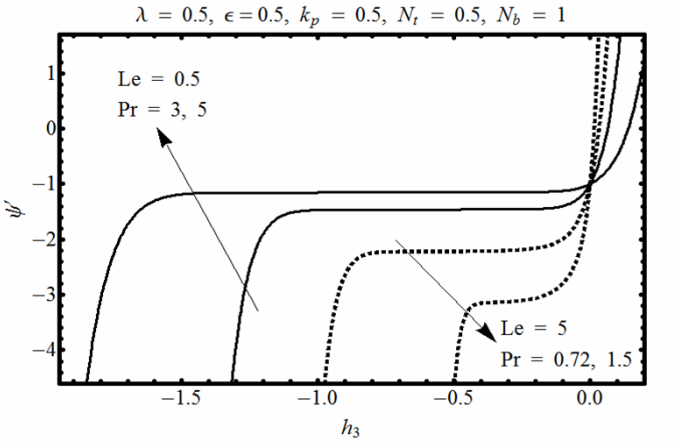

Figure 3: $\hbar$- curves for concentration profile ψ for different values of Le and Pr, plotted at 15^{th}-order of approximation

Tables 1 and 2 are presented to confirm the convergence of the obtained HAM solutions. Table 1 contains the homotopy padé approximation values for velocity, temperature and nanoparticle profiles for certain values of the involved parameters.

The padé approximates are calculated up to [20/20] approximates and the obtained values guarantee the convergence of the HAM solutions. In Table 1 padé approximations for the velocity profile calculated are for stretching ratio $\varepsilon = 0.5$, while padé accelerators for temperature and nanoparticle profiles are computed for stretching ratio $\varepsilon = 1$. It is also noticeable that convergence for velocity and temperature profiles is achieved far earlier than convergence for the nanoparticle profile. Tables 2, 3 show a comparison of the HAM and numerical solutions of the nondimensional profiles computed at the surface of the sheet. From these results both the solutions are in good agreement. Table 4 is arranged to give a comparison of the present results with the available work of Nadeem et al. [21]. From Table 4 it is obvious that the obtained values are in good agreement.

The behavior of velocity, temperature and nanoparticle profiles for different values of the involved parameters are presented in Figs. 4 to 13. Fig. 4 refers to the influence of couple stress parameter η over velocity profile f' for different values of porosity parameter k_p, when the stretching ratio $\varepsilon = 2$. From Fig. 4 it is clear that the velocity profile displays dual behavior with respect to couple stress parameter λ, namely, near the surface of the sheet the velocity

Table 3: Comparison of numerical and HAM solutions for the boundary derivatives θ' and ψ' when $\lambda = 1$, $\varepsilon = 2$, $Le = 1$, $N_b = 1$, $N_T = 0.5$

		HAM	Fehlberg	HAM	Fehlberg	HAM	Fehlberg
	$Pr\backslash k_p$	0		0.5		1.5	
$\theta'(0)$	0.7	-1.1462	-1.1462	-1.1442	-1.1442	-1.1404	-1.1404
	2.0	-1.9541	-1.9541	-1.9528	-1.9528	-1.9506	-1.9506
	7.0	-3.6688	-3.6688	-3.6681	-3.6681	-3.6668	-3.6668
	10	-4.3870	-4.3870	-4.3864	-4.3864	-4.3853	-4.3853
$\psi'(0)$	0.7	-1.6285	-1.6285	-1.6170	-1.6170	-1.5955	-1.5955
	2.0	-2.8274	-2.8274	-2.8197	-2.8197	-2.8057	-2.8057
	7.0	-5.3600	-5.3600	-5.3550	-5.3550	-5.3474	-5.3474
	10	-6.4179	-6.4179	-6.4141	-6.4141	-6.4072	-6.4072

Table 4: Comparison of present results with the results in [21]

	$\theta'(0)$					
	[21]	Present	[21]	Present	[21]	Present
$\varepsilon\backslash Pr$	0.72		1.0		10.0	
0.5	1.1663	1.1663	1.3475	1.3475	3.9196	3.9196
1.0	1.3605	1.3605	1.5960	1.5960	5.0597	5.0597
2.0	1.7040	1.7040	2.0311	2.0311	6.9145	6.9145

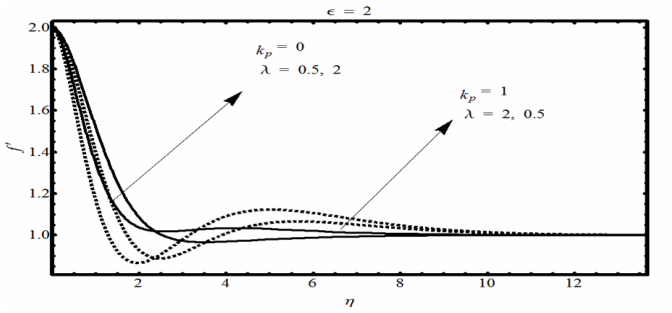

Figure 4: Influence of λ over f' for different k_p

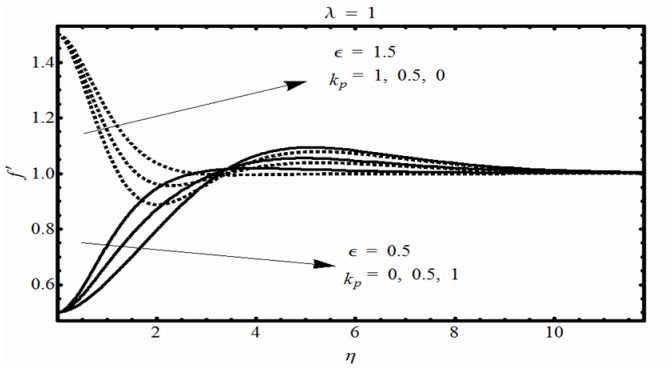

Figure 5: Influence of k_p over f' for different ε

profile increases as λ rises, while the velocity profile changes its behavior after a certain interval and then decreases as λ rises. The dual behavior is due to the fact that near the surface of the sheet, where the viscosity effects are dominant increase in couple stress λ parameter corresponds to lower viscosity and hence higher velocity profile, near the surface. In the far field region, where the viscosity effects are negligible, increase in couple stress parameter λ decreases the velocity profile due to its dependence upon the coupe stress viscosity η_0 which acts as a retarding agent and makes the fluid denser that results in a de-

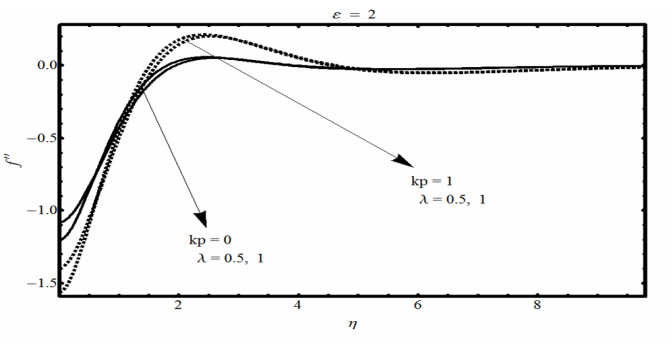

Figure 6: Influence of λ over f'' for different k_p

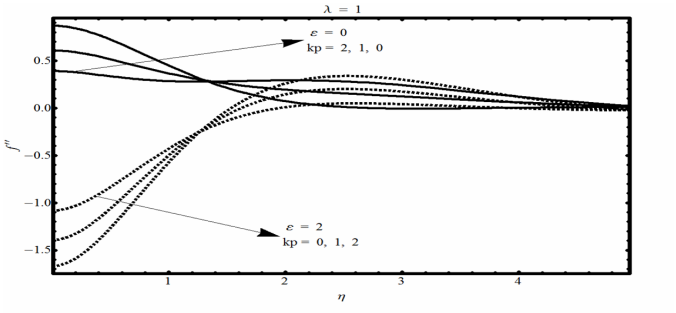

Figure 7: Influence of k_p over f'' for different ε

crease in the velocity profile. In Fig. 4 the behavior of the velocity profile is sketched when the fluid is flowing without a porous medium $\left(k_p = 0\right)$ and fluid through a porous medium with porosity parameter $k_p = 1$. It is also noted from Fig. 4 that the turning points for the velocity profile for different k_p lie almost at the same η, while the convergence rate for the velocity profile is much quicker for smaller k_p. Fig. 5 reflects the influence of porosity parameter k_p plotted for different values of stretching ratio ε, when couple stress parameter $\lambda = 1$. From Fig. 5 it is noted that the velocity profile near the sheet surface decreases with increases in porosity parameter k_p, while in the far field region the velocity profile changes its behavior and increases as k_p rises. The convergence rate for the velocity profile with $\varepsilon = 0.5, 1.5$ is almost the same. Figs. 6 and 7 gives the pattern followed by the velocity gradient for different combinations of the involved parameters that guarantees the satisfaction of the boundary conditions for the velocity gradient f'' associated with the couple stress fluid model. Fig. 6 gives the behavior of velocity gradient f'' for different values of couple stress parameter λ for fluid flowing through a porous medium with porosity parameter $k_p = 0, 1$. It is observed from Fig. 6 that near the boundary of the sheet velocity gradient f'' decreases with increase in λ while in the far field region, increase in λ increases the velocity gradient. It is also evident from Fig. 6 that increase in porosity parameter k_p increases the deviation of velocity gradient from the mean position.

Fig. 7 is plotted to observe the behavior of porosity parameter k_p for couple stress fluids with $\lambda = 1$, computed for the flat plate case ($\varepsilon = 0$), and stretching sheet problem with stretching ratio $\varepsilon = 2$. The dual

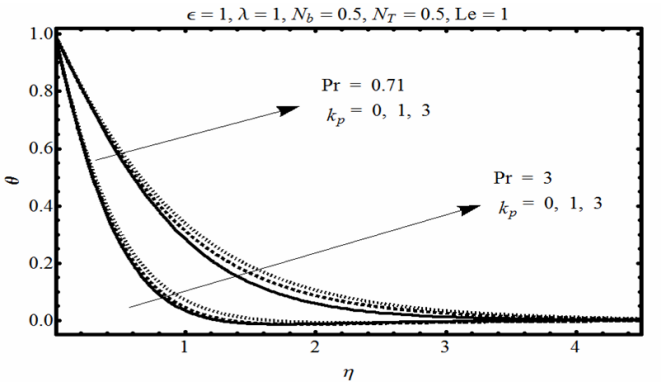

Figure 8: Influence of k_p over θ for different Pr

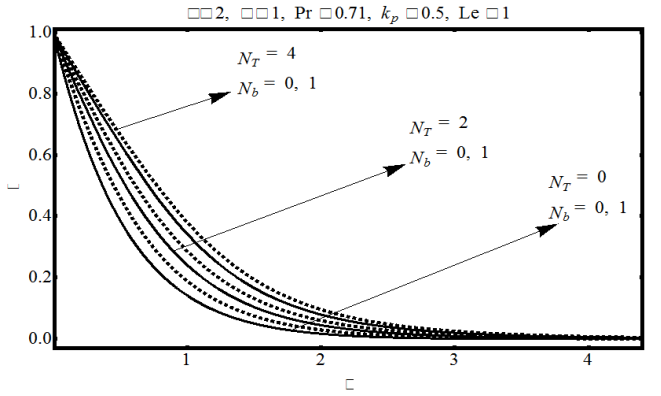

Figure 9: Influence of N_b over θ for different N_T

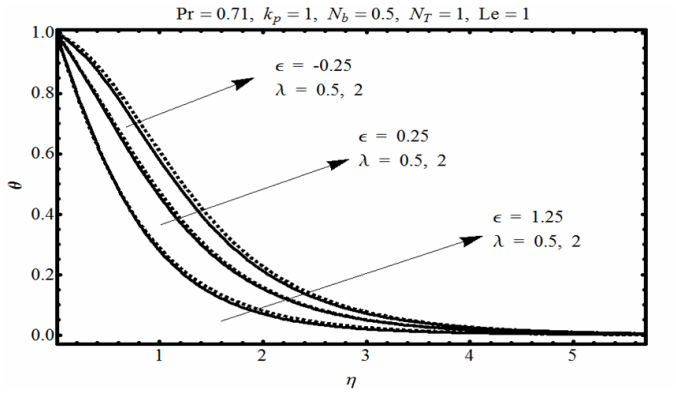

Figure 10: Influence of λ over θ for different ε

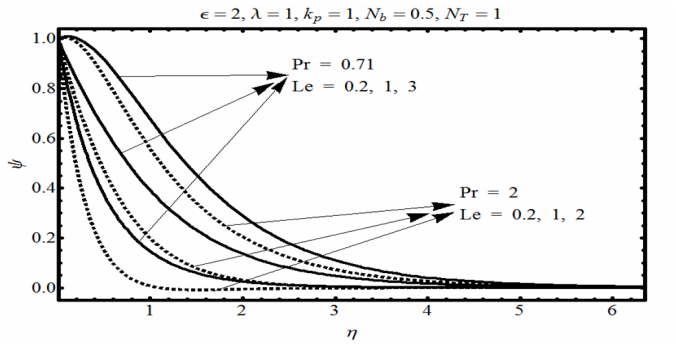

Figure 11: Influence of Le over ψ for different Pr

behavior is evident in the sketch. From Fig. 7 it is predicted that near the boundary of the sheet the velocity gradient decreases with increase in k_p, while in the far field area the velocity gradient increases with increase as k_p rises. Fig. 8 inculcates the influence of porosity parameter k_p over temperature profile θ for different values of Prandtl numbers Pr and for specified values of the other parameters. From Fig. 8 it is depicted that the influence of k_p over θ is opposite to Pr in that as Pr rises the temperature profile θ and the thermal boundary layer thickness decreases, whereas as porosity parameter k_p rises, the temperature profile increases.

Fig. 9 describes the influence of Brownian number N_b over the temperature profile computed for different values of the thermophoresis number N_T. From Fig. 9 it is observed that increases in both Brownian number N_b and thermophoresis number N_T result in the temperature profile θ increasing. This observation is consistent with the fact that nanoparticles have high thermal conductivity and so a higher heat transfer rate. Fig. 10 shows the influence of couple stress parameter λ over temperature profile θ for shrinking sheet with $\varepsilon = -0.25$ and stretching sheet with $\varepsilon = 0.25, 1.5$ for specified values of the other involved parameters. From Fig. 10 it is clear that an increase in ε decreases the temperature profile θ and the thermal boundary layer thickness, while an increase in λ increases the temperature profile θ. Fig. 11 indicates the behavior of the nanoparticle profile for different values of the Lewis numbers Le computed for different Prandtl numbers Pr.

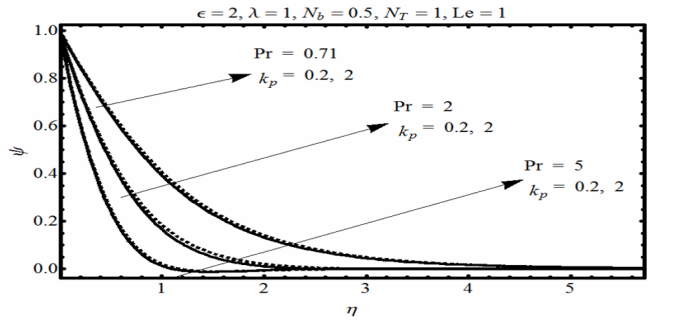

Figure 12: Influence of Pr over ψ for different k_p

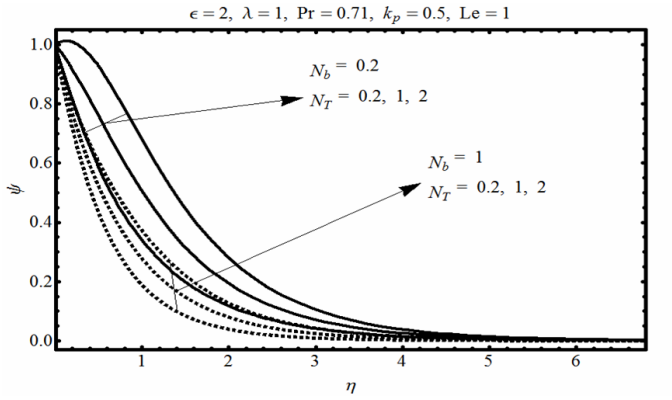

Figure 13: Influence of N_b over ψ for different N_T

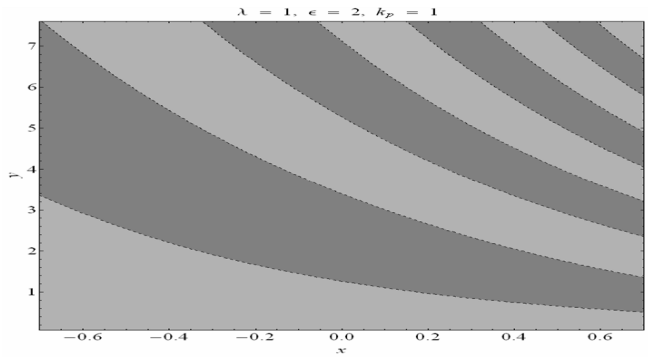

Figure 14: Behavior of streamlines for the velocity profile $f(x, y)$

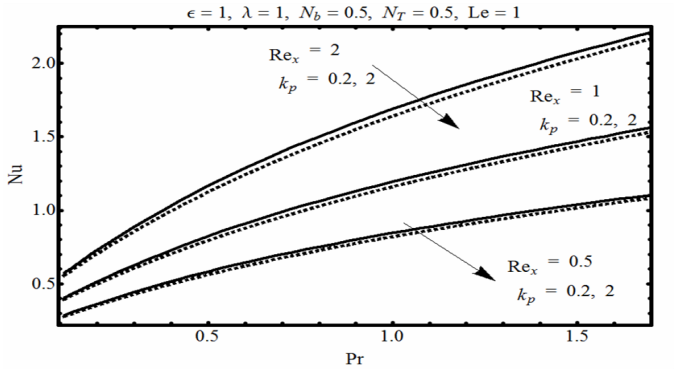

Figure 15: Influence of Re_x over Nusselt numbers Nu against Pr for different k_p

From Fig. 11 it is predictable that with an increase in both Le and Pr the nanoparticle profile and the nano boundary layer thickness decrease. Fig. 12 gives the influence of porosity parameter k_p over the nanoparticle profile calculated for different values of Prandtl number Pr. From Fig. 12 it is clear that an increase in k_p increases the nanoparticle profile. Fig. 13 is prepared to analyze the behavior of thermophoresis number N_T over the nondimensional nanoparticle profile ψ for different values of the Brownian number N_b. The sketch indicates that an increase in thermophoresis number N_T increases the nanoparticle profile ψ.

The streamline pattern associated with the velocity profile f in the (x, y) plane is shown in Fig. 14 for couple stress parameter $\lambda = 1$. The decaying pattern in streamlines is observable from the sketch. Fig. 15 shows the behavior of Nusselt numbers graphed for different porosity parameters k_p and local Reynolds numbers Re_x plotted against Prandtl numbers Pr. From Fig. 15 it is observed that with an increase in Pr and Re_x local Nusselt numbers increases, while local Nusselt numbers decreases with respect to porosity parameter k_p. Table 5 contains values for boundary derivatives for nondimensional temperature profile θ at the surface of the sheet which corresponds to the influence of heat flux at the surface of the sheet for different values of porosity parameter k_p, Prandtl numbers Pr and Brownian number N_b. From Table 5 it is noted that with an increase in Prandtl numbers Pr, heat flux at the surface increases, whereas with an increase in k_p and N_b, heat flux at the surface decreases. Table 6 refers to the behavior of Sherwood number Sh for different combinations of porosity parameter k_p, Prandtl numbers Pr and Lewis numbers Le that correspond to the mass transfer rate at the surface of the sheet. From Table 6 it is noticed that with an increase in both Pr and Le Sherwood numbers increases.

References

[1] H. Rosali, A. Ishak, I. Pop, Stagnation point flow and heat transfer over a stretching/shrinking sheet in a porous medium, Int Commun Heat Mass Tran 38 (2011) 1029–1032.

[2] I.-C. Liu, Flow and heat transfer of an electrically conducting fluid of second grade in a porous medium over a stretching sheet subject to a transverse magnetic field, Int J Non-Lin Mech 40 (2005) 465–474.

[3] S. Nadeem, M. Awais, Thin film flow of an unsteady shrinking sheet through porous medium with variable viscosity, Physics Letters A 372 (2008) 4965–4972.

[4] S. Nadeem, M. Hussain, M. Naz, Mhd stagnation flow of a micropolar fluid through a porous medium, Meccanica 45 (2010) 869–880.

[5] M. E. Ali, The effect of lateral mass flux on the natural convection boundary layers induced by a heated vertical

Table 5: Behavior of heat flux at the surface of the sheet when $\lambda = 1$, $\varepsilon = 0.5$, $k_p = 0.5$, $N_T = 0.5$, $Le = 1$

	$-\theta(0)$						
	$Pr \backslash N_b$	0.1	0.2	0.5	1.0	1.5	2.0
$k_p = 0.5$	0.7	0.85428	0.83051	0.78090	0.64500	0.53654	0.43632
	2.0	1.39052	1.36264	1.26977	1.09915	0.92758	0.76766
	7.0	2.45602	2.44693	2.29508	2.00517	1.71996	1.45353
	10	2.90465	2.86284	2.69916	2.38940	2.07920	1.75129
$k_p = 1.5$	0.7	0.82850	0.80454	0.75276	0.61787	0.51049	0.41337
	2.0	1.35848	1.32958	1.23187	1.05344	0.87921	0.72209
	7.0	2.47591	2.43351	2.26806	1.95937	1.66174	1.39104
	10	2.91600	2.86969	2.68876	2.35143	2.02038	1.75103

Table 6: Behavior of Sherwood number when $\lambda = 1$, $\varepsilon = 0.5$, $k_p = 0.5$, $N_b = 0.5$, $N_T = 1$

	$-\psi'(0)$						
	$Pr \backslash Le$	0.0	0.25	0.5	1.0	2.0	5.0
$k_p = 0.5$	0.7	0.19876	0.31113	0.41837	0.61863	0.96968	1.74583
	2.0	0.21738	0.35904	0.49709	0.89361	1.51097	2.69289
	5.0	0.24730	0.39879	0.73234	1.28213	2.08192	3.60141
	7.0	0.32979	0.62777	0.89534	1.35524	2.27060	3.87877
$k_p = 1.5$	0.7	0.18537	0.29666	0.40283	0.30102	0.94843	1.70876
	2.0	0.20616	0.33923	0.48951	0.87404	1.47847	2.65723
	5.0	0.22471	0.35607	0.71728	1.25368	2.04430	3.56893
	7.0	0.29118	0.62260	0.88176	1.32951	2.23321	3.84671

plate embedded in a saturated porous medium with internal heat generation, International Journal of Thermal Sciences 46 (2007) 157–163.

[6] E. M. A. Elbashbeshy, M. A. A. Bazid, Heat transfer in a porous medium over a stretching surface with internal heat generation and suction or injection, App Math Comp 158 (2004) 799–807.

[7] H. Rosali, A. Ishak, I. Pop, Micropolar fluid flow towards a stretching/shrinking sheet in a porous medium with suction, Int. Commun. Heat Mass Transf. 39 (6) (2012) 826–829.

[8] M. Hameed, S. Nadeem, Unsteady mhd flow of a non-newtonian fluid on a porous plate, Journal of Mathematical Analysis and Applications 325 (2007) 724–733.

[9] C. Yang, A. Nakayama, W. Liu, Heat transfer performance assessment for forced convection in a tube partially filled with a porous medium, Int. J. Ther. Sci. 54 (2012) 98–108.

[10] M. Z. Salleh, R. Nazar, I. Pop, Boundary layer flow and heat transfer over a stretching sheet with newtonian heating, J Taiwan Ins Che Eng 41 (2010) 651–655.

[11] A. V. Kuznetsov, D. A. Nield, Natural convective boundary-layer flow of a nanofluid past a vertical plate, International Journal of Thermal Sciences 49 (2) (2010) 243–247.

[12] S. Nadeem, A. Rehman, M. E. Ali, The boundary layer flow and heat transfer of a nanofluid over a vertical slender cylinder, in: Proc Ins Mec Eng Part N, J Nanoeng Nanosys JNN301R2, J Nanoeng Nanosys.

[13] S. Ahmad, I. Pop, Mixed convection boundary layer flow from a vertical flat plate embedded in a porous medium filled with nanofluids, Int Commun Heat Mass Tran 37 (2010) 987–991.

[14] Y. Xuan, W. Roetzel, Conceptions for heat transfer correlation of nanofluids, Int J Heat Mass Transfer 43 (2000) 3701–3707.

[15] S. Nadeem, A. Rehman, K. Vajravelu, J. Lee, C. Lee, Axisymmetric stagnation flow of a micropolar nanofluid in a moving cylinder, article id 378259, Mathematical Problems in Engineering 2012.

[16] S. M. S. Murshed, K. C. Leong, C. Yang, Investigations of thermal conductivity and viscosity of nanofluids, International Journal of Thermal Sciences 47 (5) (2008) 560–568.

[17] N. B. Naduvinamani, P. S. Hiremath, G. Gurubasavaraj, Effect of surface roughness on the couple-stress squeeze film between a sphere and a flat plate, Tribology International 38 (2005) 451–458.

[18] A. Noghrehabadi, R. Pourrajab, M. Ghalambaz, Effect of partial slip boundary condition on the flow and heat transfer of nanofluids water nanofluids over an isothermal stretching sheet with suction or injection, J. Comp. App. Res. Mech. Eng. 1 (2012) 35–47.

[19] A. Noghrehabadi, M. Ghalambaz, A. Ghanbarzadeh, Heat transfer of magetohydrodynamic viscous nanofluids over an isothermal stretching sheet, J. Ther. Heat Tran. 2012 (4) (26) 686–689.

[20] A. Noghrehabadi, M. Ghalambaz, M. Ghalambaz, A. Ghanbarzadeh, Comparing thermal enhancement of ag-water and sio2-water nanofluids over an isothermal stretching sheet with suction or injection, J. Comp. App. Res. Mech. Eng. 2 (1) (2012) 35–47.

[21] S. Nadeem, A. Rehman, M. Y. Malik, Boundary layer stagnation-point flow of third grade fluid over an exponentially stretching sheet, Brazilian Journal of Chemical Engineering.

[22] S. J. Liao, Beyond perturbation: introduction to the homotopy analysis method, Chapman & Hall/CRC Press, Boca Raton, 2003.

[23] R. Ellahi, Effects of the slip boundary condition on non-newtonian flows in a channel, Communications in Nonlinear Science and Numerical Simulation 14 (4) (2009) 1377–1384.

[24] A. Rehman, S. Nadeem, Mixed convection heat transfer in micropolar nanofluid over a vertical slender cylinder, 124701, Chinese Physics Letters 29 (12). doi:10.1088/0256-307X/29/12/124701.

[25] S. Nadeem, A. Rehman, C. Lee, J. Lee, Boundary layer flow of second grade fluid in a cylinder with heat transfer, article id 640289, Mathematical Problems in Engineering 2012. doi:10.1155/2012/640289.

[26] R. Ellahi, A. Raiz, Analytical solution for mhd flow in a third grade fluid with variable viscosity, Math Comp Mod 52 (2010) 1783–1793.